

FINITE ELEMENT ANALYSIS OF THREE-DIMENSIONAL RTM PROCESS

Manas K. Deb, Mahender P. Reddy, Ravisankar S. Mayavaram, and Carlos E. Baumann

The Computational Mechanics Company, Inc.

7800 Shoal Creek Blvd, Suite 290E,

Austin, TX 78757

Abstract

This paper presents the mathematical theory, computational algorithm and numerical results from a finite element based Resin Transfer Molding (RTM) model, a process that involves resin impregnation of fiber preforms. The uniqueness of the present approach is that unlike the conventional methods, it treats the flow of resin and air as a two-phase flow in a porous media. The formulations are done in 3D without introducing approximations in the thickness direction. This approach enables the user to model the macro-level physics better, simulates accurate filling of complex parts that may be thick or contain inserts, predicts air entrapment, and has the ability to incorporate heat transfer in both filled and unfilled regions.

1. Introduction

1.1 Background

RTM process is being increasingly employed for high volume production of both thin and thick fiber reinforced composites commonly used in military, aerospace and automotive industries. This process involves filling a mold with polymer resin containing a fiber preform. The curing of the resin may begin during or after the mold filling. The part is de-molded after curing. RTM provides a cost-effective alternative for manufacturing of geometrically complex parts having high strength-to-weight ratios. The process also offers high flexibility in terms of tooling, tolerances and surface quality. RTM also requires low initial investment.

In the RTM process, the mold fill and the resin cure behaviors are critical factors which are affected by the choice of mold, gate and vent locations, operating temperatures, etc. Some of the common defects in RTM processes are: dry patch, fiber washout, and void entrapment (dry spots). A thorough understanding of the sensitivity of the process to the control parameters is needed in order to optimize the manufacturing process and produce defect-free parts.

1.2 RTM Simulation: State-of-the-Art

Various micro- and macro-models have been put forward by researchers to model the resin flow through the fiber

preform. Due to the computational simplicity, macro-models have received greater attention in the numerical analysis studies. Macro models consider the propagation of the resin through the fiber preform to be the same as a fluid through a porous medium. Darcy's law, which relates the pressure gradient to the velocity, using the fiber permeability and resin viscosity, is the basis of such macro-models. A unified three-dimensional mathematical model for resin flow in various processes including resin transfer molding is presented in [1]. Simulation of isothermal filling of resin in two-dimensional cavities using finite difference (FD) and finite element control volume (FECV), are reported, for example, in [2-5]. In these cases the flow details in the thickness direction are ignored. Such strategies are inadequate for filling of thick parts or if the part geometry is complex (e.g., in presence of ribs, stiffeners, inserts, etc.). Full three-dimensional non-isothermal resin flow simulations are reported by Chang and Kikuchi [6], and Young [7], where, 3D macro-model and homogenization techniques were used, respectively. The above mentioned numerical models ignore the unfilled region of the mold during the simulation. Similar to injection molding simulation, after each time step, the moving flow front is advanced and the computational flow domain is updated. Since the air-phase in the unfilled region of the mold is not considered, these methods can not predict void entrapment. Use of porous media flow equation (i.e. Darcy relation) in three-dimensional RTM simulation have been reported, for example, in [8], where both filled and unfilled regions were modeled. However, since the velocity at the fill front is never computed, questions remain as to how to use this approach for non-Newtonian fluids and non-isothermal filling with reaction kinetics.

It is important to note that one of the primary requirements of Darcy's law is that the flowing fluid must completely saturate the porous media. Since this condition is seldom met in the vicinity of the front, modified Darcy's law [9] must be used to predict the front movement accurately. This requires the use of an effective permeability for resin and air which is a function of the saturations of each the phases. This introduces the concept of relative permeability which is defined as the ratio of the effective permeability to the absolute permeability. Modified Darcy's law is widely used in reservoir simulations [10], and have also been used in the context of finite element simulation of multi-phase flow in porous media [11].

2. Proposed Method

Resin transfer molding involves resin flow through a fiber preform. The macroscopic model we consider here models this as a two-phase flow (resin/air) through a porous media (i.e. the preform). Traditional approaches ignore the unfilled region and solve only for resin flow. The drawbacks of such assumptions are listed above. In this section we present the governing equations for two-phase flow in porous media and describe the proposed approach.

2.1 Governing Equations

Mass Conservation: In this section we describe the conservation equations and boundary conditions that govern the displacement of incompressible, immiscible two-phase (resin and air) fluids through a porous media. For this presentation, isothermal conditions are assumed and the effects of capillary pressure are ignored. Let $\Omega \subset \mathcal{R}^n$ ($n = 3$) denote the flow domain. The laws of conservation of mass for each phase (resin and air) are:

$$\partial(\phi S_i)/\partial t = -\nabla \cdot (\rho_i \mathbf{v}_i) \quad i = 1, g \quad \text{in } \Omega \quad (1)$$

$$\sum S_i = 1 \quad (2)$$

Here ϕ denotes the porosity, ρ_i , S_i , and \mathbf{v}_i are respectively the density of the fluid, phase saturation, and phase velocity vector. The subscripts l and g indicate resin and air phases, respectively. Darcy's Law relates phase velocities (\mathbf{v}_i) to phase the pressures p_i .

$$\mathbf{v}_i = -\mathbf{m}_i \nabla p_i - \rho_i g \nabla D \quad \text{in } \Omega \quad (3)$$

In the above equation, D denotes the height, and \mathbf{m}_i denotes mobility of phase i and is given by

$$\mathbf{m}_i = \mathbf{k} \quad k_{ri} / \mu_i \quad (4)$$

Here, \mathbf{k} is the absolute permeability tensor for the fiber preform, k_{ri} is the relative permeability of phase i , and μ_i is the molecular viscosity of phase i . In the case of nonisothermal flows, viscosity is a function of temperature and degree of curing.

Equations (1) - (3) can be rearranged (see [10] for details) into one parabolic equation and one essentially hyperbolic equation. The parabolic equation describes the pressure field throughout the mold cavity (pressure equation) and the hyperbolic equation governs the movement of fluid fronts through the mold cavity (saturation equation). The resulting equations for incompressible fluids are:

$$\tilde{\mathbf{N}} \cdot \mathbf{v}_t = 0 \quad \text{in } \Omega \quad (5)$$

$$\mathbf{v}_t = \mathbf{v}_l + \mathbf{v}_g \quad \text{in } \Omega \quad (6)$$

$$\phi(\partial S_l / \partial t) = \tilde{\mathbf{N}} \cdot (\mathbf{h}_l \cdot \tilde{\mathbf{N}} S_l) - \tilde{\mathbf{N}} \cdot (f_l \mathbf{v}_t) - \tilde{\mathbf{N}} \cdot (\mathbf{G}_l \cdot \tilde{\mathbf{N}} D) \quad \text{in } \Omega \quad (7)$$

where, \mathbf{v}_t is the total velocity vector, \mathbf{h}_l is the capillary term, \mathbf{G}_l and the gravity term, and are given by:

$$\mathbf{h}_l = -\mathbf{m}_g f_l (d p_c / d S_l) \quad (8)$$

$$\mathbf{G}_l = f_l (\rho_l + \rho_g) g \mathbf{m}_g \quad (9)$$

where, f_l is the fractional flow coefficient.

2.2 Boundary Conditions

To complete the set of equations, Equations (5) and (7) need to be combined with an appropriate set of boundary conditions. Let Γ be the boundary of the domain Ω . This boundary consists of the inlet gates, exit vents, and the no-flow boundary. For the pressure equation, the pressures (essential boundary condition) or the fluxes (natural boundary condition) must be specified along the boundary. For the saturation equation, only the saturation at the inlet gate boundary is specified. Let Γ_i denote the inlet vent boundary, Γ_v be the exit vent boundary, and Γ_n denote the no-flow boundary. We have $\Gamma = \Gamma_i \oplus \Gamma_v \oplus \Gamma_n$. Similarly, for the energy equation, the resin temperature at the inlet is specified, and at the mold walls either the temperature or the heat flux is specified. Mathematically, the boundary conditions are:

Pressure Equation:

$$\begin{aligned} p &= P_i & \text{or} & & \mathbf{v}_t \cdot \mathbf{n} &= Q_i & \text{on } \Gamma_i \\ p &= P_v & \text{or} & & \mathbf{v}_t \cdot \mathbf{n} &= Q_v & \text{on } \Gamma_v \\ & & & & \mathbf{v}_t \cdot \mathbf{n} &= 0 & \text{on } \Gamma_n \end{aligned}$$

Saturation Equation:

$$S = S_l = 1 \quad \text{on } \Gamma_i$$

2.3 Finite Element Model

The equations presented here have been solved using hp -finite element method. (h and p stand for size and interpolation orders of the elements, respectively.) The RTM application has been developed on an hp -finite element kernel called ProPHLEX [12]. The details are similar to those presented in [11] and are omitted here for brevity. ProPHLEX offers a variety of methods for estimation of error in the computed solution and can perform dynamic adaptivity based on such estimates. The implementation presented here is capable of mesh adaptivity which, it hoped, will further improve the solution quality for a given computational cost.

3. Results and Discussion

In this section, three problems solved to validate the model developed and to demonstrate its capabilities. The first two problems, 1-D preform filling and the filling of an annulus

with gravity assistance are taken from Voller *et al* [13]. In the third problem, filling of a 3-D coil is presented and the model captures subtle aspects of RTM like the air entrapment. The results clearly demonstrate the superior performance of the model developed.

3.1 1-D preform filling

Figure 1 shows the mesh used for the 1-D preform filling. Projection of the mesh along the flow direction is shown. The data given in [13] is used for the problem. Results compare well with the analytical solution available in [13]. Figure 2 shows the flow front location at different time steps. In figure 3, distribution of the resin saturation and the average pressure are shown. Due to the 2-phase nature of the analysis, some smearing of the flow front can be seen in the figure. The amount of smearing is proportional to the size of the mesh, in particular that of those at the resin front. The sharpness of the front improves as the mesh is refined. This indicates the potential benefit to be had from dynamic adaptivity.

3.2 Annulus filling (with gravity)

The effect of gravity will influence the filling process by skewing the flow front. Figure 4 shows the finite element mesh used for solving the filling of the annulus under gravity. Typical properties for resin and air are used, and conditions used are same as those in [13]. In figure 5 the flow front location in terms of an *equivalent radius* is compared with the numerical results available in [13] and results agree well. Figures 6 and 7 show the distribution of pressure and resin saturation in the flow field.

3.3 3-D coil filling

RTM of complex 3-D parts are prone to air entrapments and dry spots. This is critical in designing the injector and vent locations. An incorrect choice will lead to defects and high part rejection rate. An accurate two-phase, 3-D flow model is required to simulate and design these processes. Figure 8 shows the finite element mesh used for the 3-D model. Figure 9 clearly shows the air entrapment during the filling process.

4. Conclusions

Results shown here validate the model developed. It also indicates some of the advanced features of the model. We are hopeful that the present model can be used as an efficient design tool for RTM.

Acknowledgements

The examples presented here are solved using *PHLEXprocess*: a process simulation application code built on COMCO proprietary *hp*-adaptive finite element kernel *PHLEX*. The authors would like to thankfully acknowledge the help from *PHLEX* kernel group.

References

1. Dave, R., *J. Composite Materials*, **Vol. 24**, pp. 22-41, (1990).
2. Advani, S. G., Brusckhe, M. V., and Parnas, R., in *Flow and rheology in polymer composite manufacturing*, S. G. Advani., (ed). pp. 465-516, Elsevier, Amsterdam, (1994).
3. Brusckhe, M. V., and Advani, S. G., *ANTEC 89*, pp. 1769-1773 (1989).
4. Carpenter, G., Leek, R., Donnellan, T., and Rubel, A., in *Heat and Mass Transfer in Materials Processing and Manufacturing HTD-261*, ASME, pp. 133-145, (1993).
5. Coulter, J. P., Güçeri, S. I., *J. Reinforced Plastics and Composites*, **Vol. 7**, pp. 200-219, (1988).
6. Chang, W., and Kikuchi, N., *Computational Mechanics*, **Vol. 16**, pp. 22-35, (1995).
7. Young, W. B., *J. Composite Materials*, **Vol. 28, No. 12**, pp. 1098-1113, (1994).
8. Mohan R. V., Ngo, N. D., and Tamma, K. K., *AIAA Aerospace Science Meeting and Exhibit*, (1996). [24]
9. Muskat, M., and Meres, A. W., *Physics*, **Vol. 7**, (1936).
10. Peaceman D. W., *Fundamentals of numerical reservoir simulation*, Elsevier, Amsterdam, (1977).
11. Deb, M. K., Reddy, M. P., Thuren, J. B., and Adams, W. T., *SPE 70th Annual Technical Conference and Exhibition*, Oct. 22 - 25, 1995, Dallas, TX.
12. ProPHLEX: An *hp*-Adaptive Finite Element Kernel, Computational Mechanics Company (1996).
13. Voller, V.R., Peng, S and Chen, Y.F, *International Journal for Numerical Methods in Engineering*, **Vol. 39**, pp. 2889-2906, (1996).

Keywords

Resin transfer molding, two phase flow, finite elements

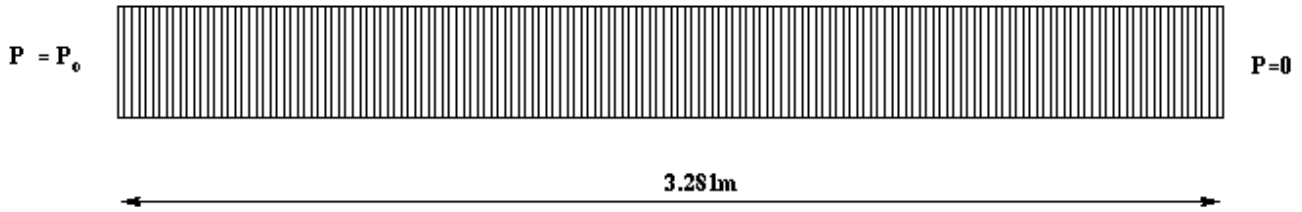


Figure 1: Finite element mesh used for the 1-D preform. Element spacing in the direction of flow is shown.

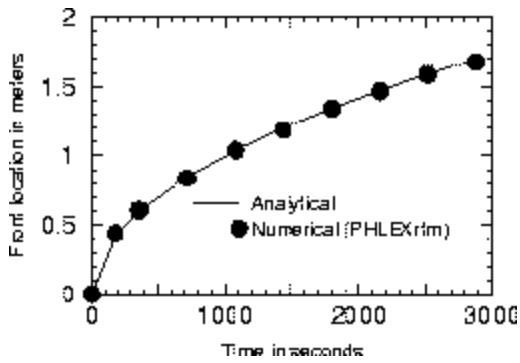


Figure 2: Comparison of the flow front location with analytical results [13] for the 1-D preform.

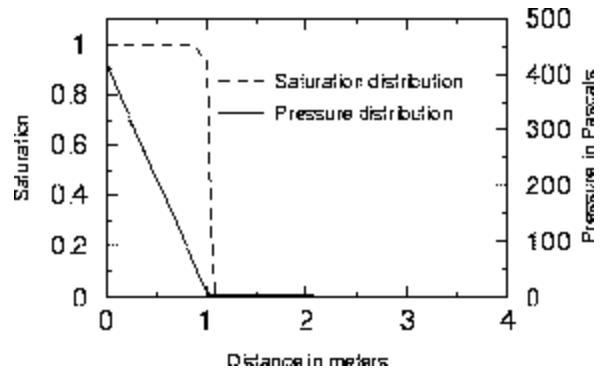


Figure 3: Distribution of saturation and pressure after 1620s in the 1-D preform

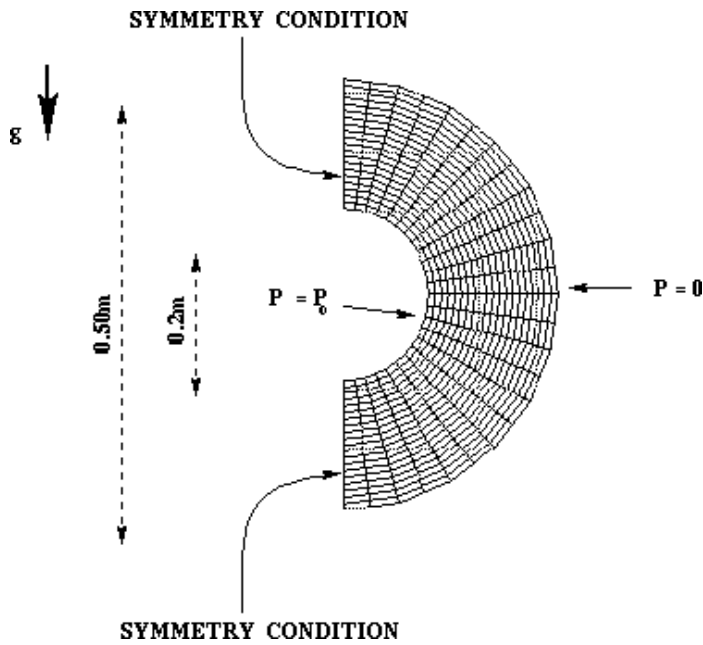


Figure 4: Finite element mesh used for RTM filling of a circular pipe under gravity.

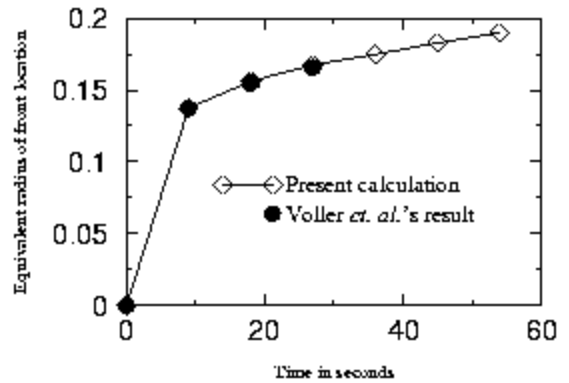


Figure 5: Comparison of the flow front location with numerical results of Voller *et al* [13].

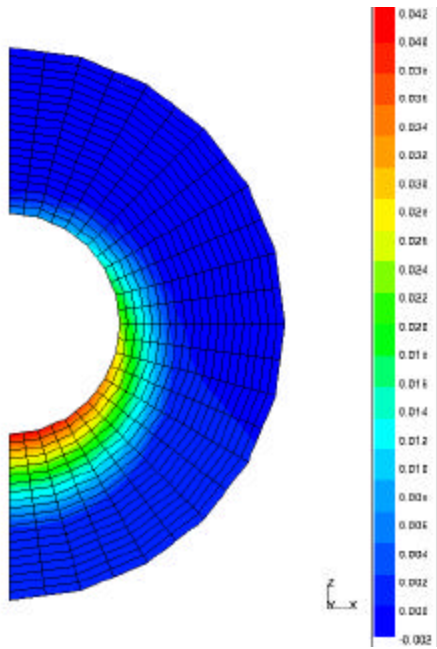


Figure 6: Distribution of pressure after 27 seconds.

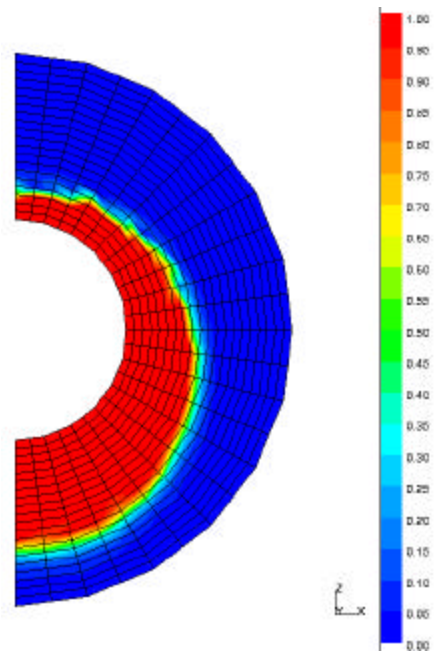


Figure 7: Distribution of saturation after 27 seconds.

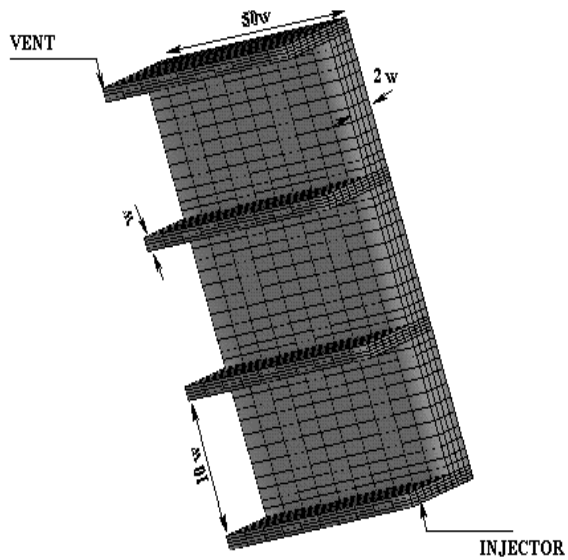


Figure 8: Finite element mesh for FTM filling of the 3-D coil.

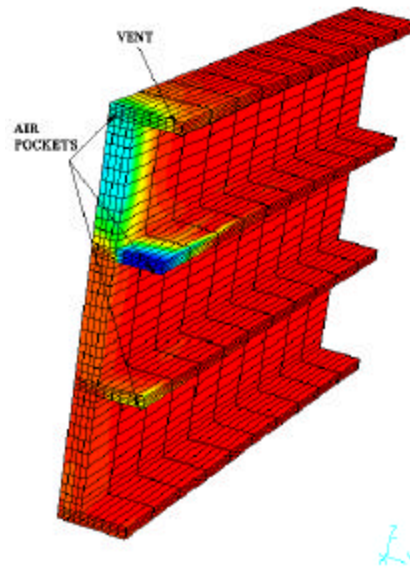


Figure 9: Distribution of saturation in the 3-D coil after 18000 seconds.